Tetrahedron 69 (2013) 2124–2130

Contents lists available at SciVerse ScienceDirect

Tetrahedron

journal homepage: www.elsevier.com/locate/tet

Synthesis of metal-free organic dyes containing tris(dodecyloxy)phenyl and dithienothiophenyl units and a study of their mesomorphic and photovoltaic properties

Muthaiah Shellaiah [a], Hsiao-Ping Fang [a], Yu-Ling Lin [a], Ying-Chan Hsu [b], Jiann-T'suen Lin [b], Hong-Cheu Lin [a,*]

[a] Department of Materials Science and Engineering, National Chiao Tung University, Hsinchu 30049, Taiwan, ROC
[b] Institute of Chemistry, Academia Sinica, Taipei, Taiwan, ROC

ARTICLE INFO

Article history:
Received 26 October 2012
Received in revised form 2 January 2013
Accepted 4 January 2013
Available online 11 January 2013

Keywords:
3,4,5-Tris(dodecyloxy)phenyl
Dye-sensitized solar cell
Dithienothiophene
Metal-free organic dye

ABSTRACT

In this study we synthesized three metal-free organic dyes (**Cpd11**, **Cpd16**, and **Cpd22**) featuring 3,4,5-tris(dodecyloxy)phenyl and cyanoacrylic acid moieties as electron-donor and electron-acceptor/anchoring units, respectively, linked through various dithienothiophenyl conjugated spacers. **Cpd16** exhibits mesomorphic properties, confirmed through polarizing optical microscopy, differential scanning calorimetry, and X-ray diffraction (XRD), due to the appropriate ratio of the lengths of its flexible chain to its rigid core. Molecular modeling of **Cpd16**, and its *d*-spacing determined from XRD data, verified the existence of a tilt angle in the SmC phase. Among these metal-free organic dyes, a dye-sensitized solar cell incorporating **Cpd16** exhibited the best performance, presumably because of its better packing and its mesomorphic properties; the power conversion efficiency was 3.72% (V_{oc}=0.58 V; J_{sc}=9.98 mA cm^{-2}; *FF*=0.65) under simulated AM 1.5 irradiation (100 mW cm^{-2}).

1. Introduction

The development of novel materials for use in organic optoelectronic devices, such as dye-sensitized solar cells (DSSCs),[1] has become a popular research topic in the quest for low-cost, green materials for sustainable use and a decrease in demand for fossil fuels and nuclear power. DSSCs based on Ru-photosensitizers,[2,3] such as *cis*-bis(isothiocyanato)bis(2,2′-bipyridyl-4,4′-dicarboxylato)-ruthenium(II) (**N3**)[4] and related derivatives, have been applied very successfully with high power conversion efficiencies (PCEs) of 9–12%.[4–9] Recently, it has been demonstrated that DSSCs can also be constructed from metal-free organic dyes.[10] Because of the high cost of rare Ru metal and the relatively low molar extinction coefficients and tedious purification of Ru-photosensitizes,[5] metal-free organic sensitizers have become increasingly attractive and widely developed.[11,12] Nevertheless, the ability to reach higher efficiencies when using metal-free organic dyes remains a challenge, although great progress has been made in this field.[13–16] The key characteristics for a dye to be used in a DSSC are high absorption over a wide range of the solar spectrum with high molar extinction coefficients, efficient charge separation, redox stability, and suitable functional groups to interact with the electron sink (TiO_2). Metal-free organic dyes featuring a donor/acceptor structural design were synthesized have particularly wide absorption ranges for DSSC applications.[11–19] Liquid-crystalline (or mesomorphic) properties can be introduced to organic dyes when 3,4,5-tris(dodecyloxy) phenyl segments are incorporated, resulting in potential applications in flexible electronic materials.[20–25] Kato et al.[21] reported conjugated oligothiophene-based polycatenar liquid crystal materials exhibiting electrochromism upon applying an oxidative potential, with layered smectic and columnar structures capable of enhancing hole mobilities up to 0.01 cm^2 V^{-1} s^{-1}. Park et al.[22] also reported that the mesomorphic organization of a dicyanodistyrylbenzene-based molecule could improve its fluorescence-emitting and semiconducting properties. Therefore, great efforts have been taken toward the preparation and characterization of photo- and electro-active structures based on mesogenic units. The use of various aromatic segments (e.g., fluorene,[26,27] thiophene[28,29]) as spacers in organic dyes can improve the photocurrent generation and intramolecular charge separation. Dithieno[3,2-*b*:2′,3′-*d*]thiophene (DTT)-conjugated dyes have also exhibited excellent DSSC efficiencies.[30] In addition, the DTT unit—a sulfur-rich (three S atoms) and electron-rich building block—increases the planarity of the dye, resulting in longer π-conjugation.[31,32] Because of restricted intramolecular rotation in fused-ring structures, such as DTT, π-orbital overlap in such conjugated molecules could be maximized to

* Corresponding author. Tel.: +886 3 5712121x55305; fax: +886 3 5724727; e-mail address: linhc@mail.nctu.edu.tw (H.-C. Lin).

0040-4020/$ – see front matter © 2013 Elsevier Ltd. All rights reserved.
http://dx.doi.org/10.1016/j.tet.2013.01.009

enhance intermolecular charge transport.[33,34] In this study, we prepared dyes featuring a 3,4,5-tris(dodecyloxy)phenyl unit[21] and a cyanoacrylic acid as electron donor and acceptor units, respectively, with various spacers inserted as the conjugated bridge (Fig. 1). For example, we introduced a fused-DTT unit as a conjugated spacer through which electrons could be transferred efficiently from the donor to the acceptor. In addition to the DTT unit (as a main structure of the conjugated spacer), we also employed bithiophene and bithiazole units to extend the conjugated lengths and, thereby, affect the electron mobilities and absorption spectra. Furthermore, bithiophene unit enhanced the liquid crystallinity of the dye. To increase solubility, we inserted alkyl chains onto bithiazole heterocyclic rings. We were aware, however, that the presence of thiophene rings in the electron-rich segment might not result in sufficient separation between the highest occupied molecular orbital (HOMO) and lowest unoccupied molecular orbital (LUMO); in addition, too many alkyl chains would affect the packing between the layers the molecule, induce molecular aggregation, increase steric hindrance, and decrease charge transfer. If the structure had too many rigid rings, however, its solubility would be impacted, making it harder to dissolve in common solvents with low boiling points and, thereby, complicating device fabrication. Therefore, we also compared the effects of bithiophene[35–37] and bithiazole[38] units. The design of the conjugated system can not only affect the absorption range but also further influence the electron transfer from the excited state to the TiO_2.[39] In this study, we suspected that better molecular arrangements and stacking would result if the donor/acceptor molecules exhibited enhanced liquid crystallinity Therefore, we prepared series of metal-free organic dyes containing DTT[37] units with good coplanarity and investigated their mesomorphic and photovoltaic properties.

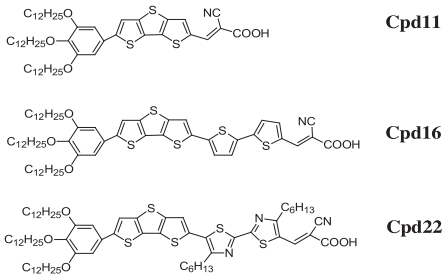

Fig. 1. Chemical structures of the dyes **Cpd11**, **Cpd16**, and **Cpd22**.

2. Results and discussion

2.1. Optical properties

Fig 2 displays the UV–vis absorption and normalized photoluminescence (PL) spectra of **Cpd11**, **Cpd16**, and **Cpd22** as solutions in THF (10^{-5} M); Table 1 lists their corresponding data. The absorption spectra reveal that the signals for **Cpd16** and **Cpd22** were red-shifted relative to those of **Cpd11** after the insertion of the bithiophene and bithiazole units, respectively, to lengthen the conjugated linking structures. The maximum absorption peaks for **Cpd11**, **Cpd16**, and **Cpd22** at 443, 476, and 473 nm, respectively, resulted from intramolecular charge transfer (ICT); that is, for the transition from the 3,4,5-tris(dodecyloxy)benzene donor to the cyanoacrylic acid acceptor. The spectra of the dyes **Cpd16** and **Cpd22** both featured weak π–π* transition bands, at 386 and 374 nm, respectively, whereas that of **Cpd11** featured only a single intense band at 443 nm (see Table 1). As expected, the elongated π-conjugations in **Cpd16** and **Cpd22** resulted in narrower π–π* energy gaps and spectral red shifts for the π–π* transitions. Because the inserted bithiophene and bithiazole units extended the

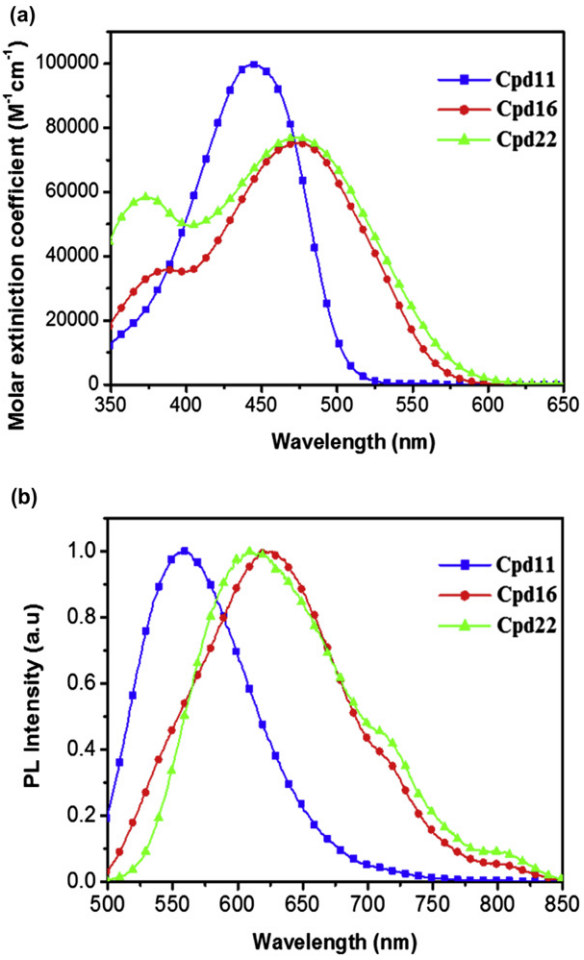

Fig. 2. (a) UV–vis absorption spectra and (b) normalized photoluminescence (PL) spectra of metal-free organic dyes in THF solutions (10^{-5} M).

Table 1
Absorption, emission, and electrochemical properties of the tested dyes

Dye	λ_{abs} (nm)[a] [ε (M^{-1} cm^{-1}]	λ_{PL}[a] (nm)	Stokes Shift[b] (nm)	E_g[c] (eV)	E_{ox}[d] (V)	HOMO[e] (eV)	LUMO[f] (eV)
Cpd11	443 (99,000)	557	114	2.45	1.15	−5.70	−3.25
Cpd16	386 (35,700) 476 (75,000)	624	149	2.19	0.71	−5.26	−3.07
Cpd22	374 (58,000) 473 (77,000)	610	135	2.15	0.77	−5.32	−3.17

[a] Absorption and PL emission wavelengths recorded in dilute THF solution (10^{-5} M) at room temperature.
[b] Stokes shift calculated from the difference between λ_{abs} and λ_{PL}.
[c] Optical band gap obtained from the equation $E_g^{opt}=1240/\lambda_{onset}$.
[d] E_{ox} is the oxidation potential.
[e] $E_{HOMO}=[-(E_{ox}-0.25)-4.8]$ eV, where 0.25 V is the value for ferrocene versus Ag/Ag+ and 4.8 eV is the energy level of ferrocene below the vacuum.
[f] $E_{LUMO}=E_{HOMO}-E_g$.

conjugation lengths in **Cpd16** and **Cpd22**, both dyes exhibited red-shifted and broader absorptions than those of **Cpd11**.[40] Since **Cpd11** had the narrowest absorption wavelength (Fig. 2a), it also displayed the worst photovoltaic performance among the tested dyes. The molar extinction coefficients of **Cpd16** (476 nm; ε=7.50×10^4 M^{-1} cm^{-1}) and **Cpd22** (473 nm; ε=7.70×10^4 M^{-1} cm^{-1}) at their maximum absorptions are lower than that of **Cpd11** (443 nm; ε=9.90×10^4 M^{-1} cm^{-1}), because the inserted bithiophene and bithiazole units decreased the coplanarity of the acceptor and

donor moieties and, therefore, decreased the degree of charge transfer.[41,42] Furthermore, in comparison with conventional ruthenium complexes (e.g., **N3**; ε=1.52×10^4 M^{-1} cm^{-1}),[4] the molar extinction coefficients of the dyes are relatively large, indicating that they have good light harvesting ability. The bathochromic shifts upon proceeding from **Cpd11** to **Cpd16** (33 nm) and from **Cpd11** to **Cpd22** (30 nm) presumably resulted from the extended π-conjugations. Fig. 2b reveals that when THF solutions of **Cpd11**, **Cpd16**, and **Cpd22** were excited at 443, 475, and 475 nm, respectively, the resulting PL spectra featured weak emissions with Stokes shifts in the range 114–148 nm, with the PL emissions of dyes following similar trends to those in their absorption spectra.

2.2. Electrochemical properties

The electrochemical properties of dyes can be obtained using cyclic voltammetry (CV); Table 1 and Fig. 3 present the relevant CV data and representative cyclic voltammograms, respectively, for **Cpd11**, **Cpd16**, and **Cpd22**. We determined the HOMO energy levels of these dyes from their corresponding irreversible oxidation peaks. The cyclic voltammograms of the dyes **Cpd11**, **Cpd16**, and **Cpd22** featured irreversible oxidation waves with oxidation potentials of 1.15, 0.71, and 0.77 V, respectively (Fig. 3). The HOMO energy level of a dye must be more positive (>0.3 eV) than the electrolyte iodine redox potential if it is to accept electrons effectively.[43–46] The HOMO energy levels of our dyes were in the range from −5.70 to −5.26 eV with respect to the I^-/I_3^- redox couple (−4.60 eV vs vacuum). Because of the absence of reduction peaks, we could not determine the LUMO energy levels of these dyes from the CV traces, but we could elucidate them by subtracting the optical band gaps from the HOMO energy levels. The resulting LUMO energy levels, in the range from −3.07 to −3.25 eV, are higher than the conduction band edge (−4.0 eV vs vacuum); therefore, the electron injection process is energetically favorable. Relative to **Cpd11** (containing only a simple fused dithienothiophene spacer), the dyes **Cpd16** (with one more bithiophene unit) and **Cpd22** (with one more bithiazole unit) both had smaller oxidation potentials (E_{ox}). Therefore, the shortest spacer in **Cpd11** (possessing the shortest conjugation length) resulted in it having the highest oxidation potential and the largest optical band gap (E_g) among our tested dyes. The optical band gaps of **Cpd11**, **Cpd16**, and **Cpd22** were 2.45, 2.19, and 2.15 eV, respectively, which suggested that **Cpd22** possibly might have a higher PCE value. However, in contrast to **Cpd11** (without a donor bithiophene linkage) and **Cpd22** (with an acceptor bithiazole linkage), the improved electron injection of **Cpd16** might be arisen from the donor bithiophene linkage and hence to achieve a higher PCE value. On the other hand, since the HOMO and LUMO levels of **Cpd16** obtained from CV measurements were found to be higher than those of **Cpd11** and **Cpd22** in Table 3, and hence a greater electron injection process was favorable to obtain a higher PCE efficiency in later photovoltaic measurements.

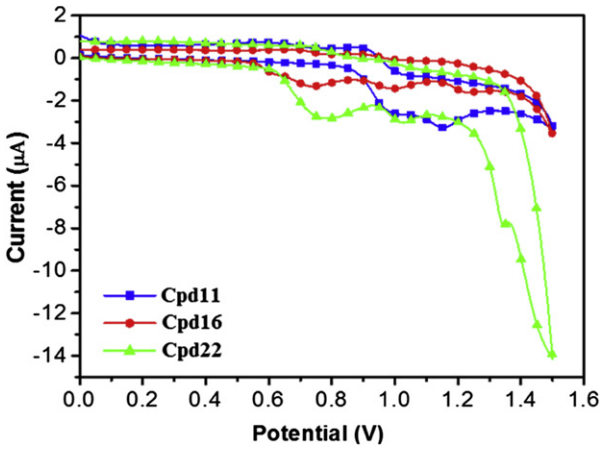

Fig. 3. Cyclic voltammograms of the dyes **Cpd11**, **Cpd16**, and **Cpd22** (in THF), recorded at a scan rate of 100 mV s^{-1}.

2.3. Mesomorphic properties

Table 2 lists the phase transition temperatures and enthalpies of the dyes **Cpd11**, **Cpd16**, and **Cpd22**, as characterized using differential scanning calorimetry (DSC). The polarizing optical microscopy (POM) image in Fig. 4 reveals that **Cpd16** possessed a tilted

Table 2
Phase transition temperatures and enthalpies of the dyes **Cpd11**, **Cpd16**, and **Cpd22**

	Phase transition (°C, [ΔH (J g^{-1})])[a,b]
Cpd11	Heating Cr_1 105.83[3.67] Cr_2 155.7[6.01] Cr_3 165.65[8.3]Iso Cooling Iso 146.21[7.88] Cr_3 130.46[1.9] Cr_2 87.83[3.17] Cr_1
Cpd16	Heating Cr_1 182.99[4.9] Cr_2 218.12[19.34] SmC 242.52[2.01]Iso Cooling Iso[c]235.2 SmC 175.10[2.04] Cr_2 142.78[1.54] Cr_1
Cpd22	Heating Cr 202.91[4.7]Iso Cooling Iso 194.97[3.3] Cr

[a] Data determined through DSC from second heating/first cooling run at a scanning rate of 5 °C min^{-1}.
[b] Abbreviations: Cr_{1-3}, different crystalline modifications; SmC, tilted smectic phase; Iso, isotropic liquid state.
[c] Isotropic temperature determined through POM.

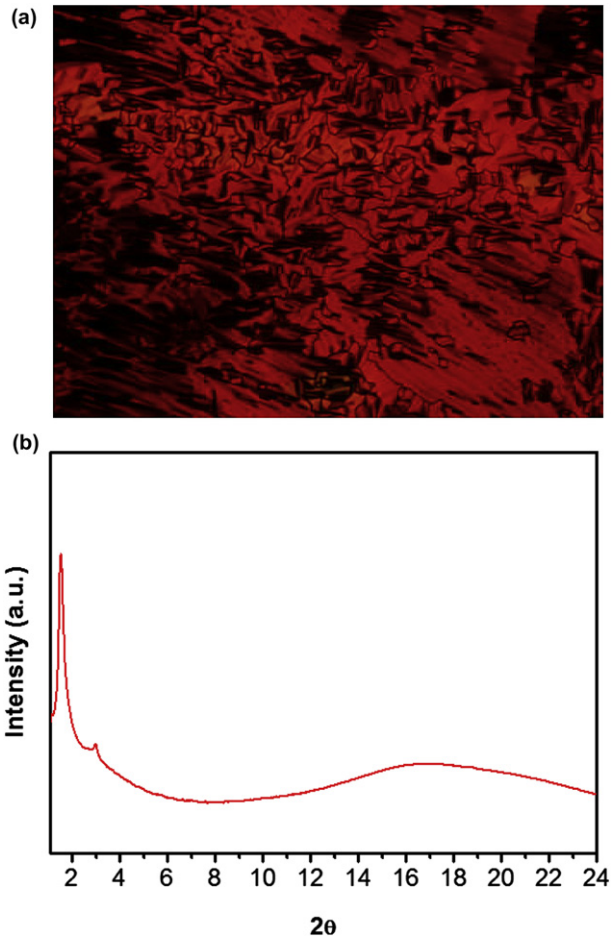

Fig. 4. (a) Optical texture of the nematic phase in the dye **Cpd16** at 225 °C (cooling), observed through POM, and (b) XRD intensity plotted with respect to angle for the dye **Cpd16** at 225 °C.

smectic (SmC) phase, with a broken focal conic fan texture at 225 °C. The mesomorphic properties of **Cpd16** were confirmed using powder X-ray diffraction (XRD); after thermal annealing at 225 °C for 10 min, **Cpd16** exhibited a primary diffraction feature in the low angle region of Fig. 4, with a sharp peak at a value of 2θ of 1.3° (corresponding to a *d*-spacing of 50.6 Å). Fig. 5 presents a possible packing motif (side-view) for **Cpd16**; this model suggests that the dye molecules stacked with bilayer packing and may have trivial interdigitated arrangements as a result of hydrogen bonding interactions between terminal carboxyl (COOH) units. Using Chemdraw software for simulation, we calculated the theoretical molecular length of **Cpd16** to be 38.44 Å; its hydrogen-bonded dimer would, therefore, have a length of ~75 Å. The *d*-spacing of 50.6 Å for **Cpd16**, determined using XRD, suggested a tilted smectic molecular arrangement (e.g., SmC phase) in Fig. 5. The broad peak in the wide angle region at a value of 2θ of 15° in Fig. 4 corresponds to a *d*-spacing of 4.6 Å, which we assign to the lateral distance between the conjugated backbones, as has been reported for other similar π-conjugated polymers presenting long pendants,[47–49] although this broad peak might also have contained some contributions from the lateral π–π stacking of the dye planes.[50] The broad XRD halos in Fig. 4 suggest, however, that π–π stacking in **Cpd16** occurred only in very small areas; that is, it mainly possessed an amorphous structure.[51]

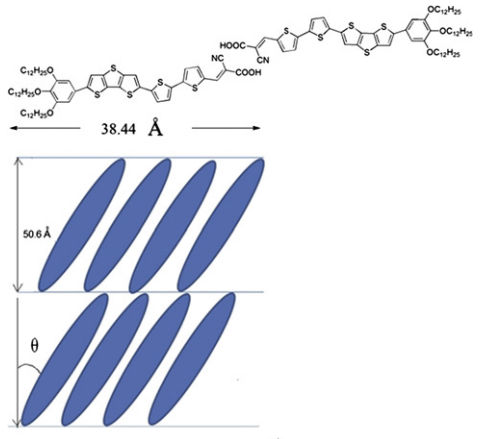

Fig. 5. Molecular model of the dye **Cpd16**.

2.4. Photovoltaic properties of DSSCs

Fig. 6 displays incident photon-to-current conversion efficiency (IPCE) and photocurrent–voltage (*I*–*V*) curves of DSSCs based on the dyes **Cpd11**, **Cpd16**, **Cpd22**, and N719. From Fig. 6b, we characterized the photovoltaic parameters of the DSSCs (Table 3), namely their open-circuit photovoltages (V_{OC}), short-circuit photocurrent densities (J_{SC}), fill factors (*FF*s), and solar-to-electrical energy conversion efficiencies (η). The power conversion efficiencies (PCEs, i.e., η) followed the trend **Cpd16** (η=3.72)>**Cpd22** (η=2.82)>**Cpd11** (η=2.69). The highest PCE was that of the DSSC incorporating **Cpd16**, mainly because it had the highest short current density (J_{sc}=9.98 mA cm^{-2}), which reveals more electrons were transferred from the excited state of the dye and injected into the conduction band of TiO_2; the DSSCs incorporating the three dyes each had similar values of V_{oc} and *FF*. The IPCE spectrum of **Cpd16** (Fig. 6a) featured the broadest response in the range 300–750 nm with a maximum IPCE value of 64%; this behavior is consistent with its DSSC having the highest PCE (η=3.72; with V_{OC}=0.58 V; J_{SC}=9.98 mA cm^{-2}; and *FF*=0.65). Thus, the highest PCE (η=3.72) for the device incorporating **Cpd16** resulted from its

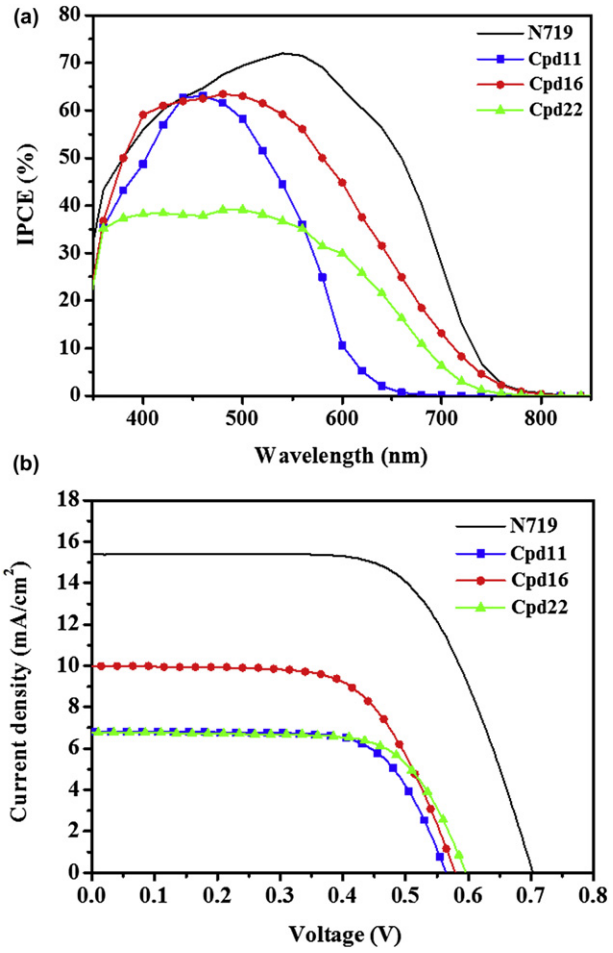

Fig. 6. (a) IPCE plots and (b) *I*–*V* curves of DSSCs fabricated using the dyes **Cpd11**, **Cpd16**, **Cpd22**, and **N719**.

Table 3
Cell performance of **Cpd11**, **Cpd16**, **Cpd22**, and **N719**-sensitized solar cells

DSSC dye[a]	V_{oc} (V)	J_{sc} (mA cm^{-2})	*FF* (%)	η (%)
Cpd11	0.57	−6.85	0.70	2.69
Cpd16	0.58	−9.98	0.65	3.72
Cpd22	0.60	−6.77	0.70	2.82
N719	0.70	−15.41	0.65	7.04

[a] Measured under AM 1.5 irradiation, 100 mW cm^{-2}.

high short current intensity (J_{sc}=9.98 mA cm^{-2}) and broadest and most-intense IPCE spectrum (toward the longer wavelength region), both of which presumably resulted from the longer conjugated structure induced by this dye's additional bithiophene linker. The different PCE values of **Cpd11**, **Cpd16**, and **Cpd22** may be attributed to the following reasons; (i) **Cpd16** and **Cpd22** were bridged through a donor bithiophene linkage and an acceptor bithiazole linkage, respectively, in contrast to **Cpd11**; (ii) the steric effect induced by the lateral alkyl chains of the bithiazole (a) unit might affect the conjugation of **Cpd22**; (iii) as noticed in Fig. 4, the greater packing nature of **Cpd16** enhanced the electron injection to TiO_2 and also enhanced J_{SC} to obtain a higher PCE value.

3. Conclusion

We have synthesized three new metal-free organic dyes (**Cpd11**, **Cpd16**, and **Cpd22**), each featuring a tris(dodecyloxy)phenyl moiety (a common unit in liquid crystalline structures) as an electron

donor, a cyanoacrylic acid moiety as an electron acceptor/anchoring group, and a DTT-based spacer to bridge the donor and acceptor moieties. To extend the length of conjugation, we appended a bithiophene or bithiazole moiety to the DTT unit to enhance the capacity for charge transfer and increase the range of absorption. The dye **Cpd16** exhibited mesomorphic properties, resulting from the appropriate ratio of the lengths of its flexible chain to its rigid core; molecular modeling of **Cpd16**, and its *d*-spacing value determined using XRD, verified the existence of a tilt angle in the SmC phase. In addition, among the tested dyes, the DSSC exhibiting the best performance was that incorporating **Cpd16**, presumably because of its superior packing as a result of its mesomorphic properties. This DSSC exhibited a maximum PCE of 3.72% (V_{oc}=0.58 V; J_{sc}=9.98 mA cm^{-2}; *FF*=0.65) under simulated AM 1.5 irradiation (100 mW cm^{-2}).

4. Experimental section

4.1. General information

4.1.1. Materials. Chemicals and solvents were of reagent grade and purchased from Aldrich, ACROS, TCI, or Lancaster Chemical. Toluene, tetrahydrofuran (THF), dimethylformamide (DMF), and dichloromethane (DCM) were dried and distilled prior to use. *N*-Bromosuccinimide (NBS) was recrystallized from distilled water and dried under vacuum. All other chemicals were used without further purification. The synthetic routes for all dyes are presented in Scheme 1. 1-Bromo-1,2,3-tris-*n*-dodecyloxybenzene (**1**),[15] tri-*n*-butyl(dithieno[3,2-*b*:2′,3′-*d*]thiophen-2-yl)stannane (**2**),[32] 5-(5-bromothiophen-2-yl)thiophene-2-carbaldehyde (**6**),[11,27] and 2-(5-bromo-4-hexylthiazol-2-yl)-4-hexylthiazole-5-carbaldehyde (**7**)[26,43] were synthesized according to literature procedures.

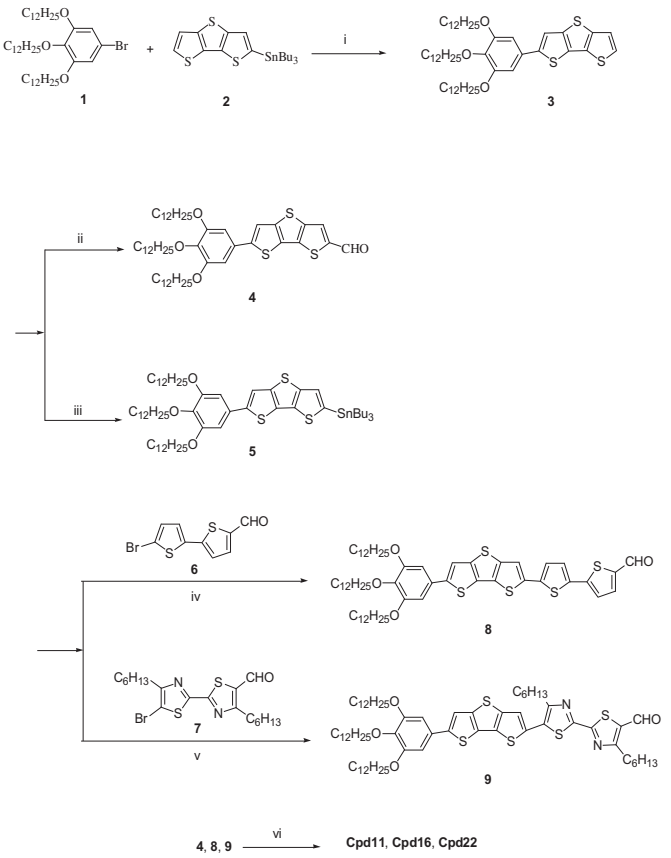

Scheme 1. Synthetic routes of dyes. (i, iv, v) $Pd(PPh_3)_4$, toluene, reflux. (ii) $POCl_3$, DMF, DCE. (iii) *n*-BuLi, THF, −78 °C, $SnBu_3Cl$. (vi) $NCCH_2COOH$, NH_4OAc, CH_3COOH.

4.1.2. Synthesis

*4.1.2.1. 2-(3,4,5-Tris-n-dodecyloxyphenyl)dithieno[3,2-b:2′,3′-d] thiophene (**3**).* A solution of **1** (2.34 g, 1.00 mmol) and **2** (1.60 g, 3.29 mmol) in dry toluene (50 mL) in a 100-mL, three-neck, round-bottom flask was deoxygenated with N_2 for 30 min. $Pd(PPh_3)_4$ (110 mg, 0.02 mmol) was added and then the mixture was heated at 110 °C for 2 days. The organic layer was extracted with DCM; the extracts were dried over anhydrous $MgSO_4$. Column chromatography (SiO_2; hexanes/CH_2Cl_2, 3:1) provided the title compound (55.6%).

*4.1.2.2. 6-[3,4,5-Tris(dodecyloxy)phenyl]dithieno[3,2-b:2′,3′-a] thiophene-2-carbaldehyde (**4**).* A 250-mL three-neck flask containing anhydrous DMF (0.1 mL, 1 mmol) was cooled in an ice bath and then $POCl_3$ (0.1 mL, 5 mmol) was added dropwise over 30 min. A solution of **3** (0.82 g, 0.1 mmol) in 1,2-dichloroethane (30 mL) was added to the solution and then the mixture was heated at 90 °C for 24 h. This solution was cooled to room temperature, poured into ice water, and neutralized to pH 6–7 through dropwise addition of saturated aqueous NaOH. The mixture was partitioned between CH_2Cl_2 and water. The organic layer was dried ($MgSO_4$) and concentrated under reduced pressure. The crude product was purified through column chromatography SiO_2; (CH_2Cl_2/hexane, 1:1) to give a yellow solid (0.7 g, 82%).

*4.1.2.3. 6-[3,4,5-Tris(dodecyloxy)phenyl]-2-tributylstannyl dithieno [3,2-b:2′,3′-a]thiophene (**5**).* *n*-BuLi (2.5 M in hexane, 0.59 mL, 1.5 mmol) was added over 1 h to a stirred solution of **3** (0.83 g, 0.1 mmol) in dry THF (20 mL) in a 250-mL flask at −78 °C. The mixture was then warmed slowly (1 h) to room temperature under an ambient environment with stirring. After the mixture was had been re-cooled to −78 °C, Bu_3SnCl (0.53 mL, 1.2 mmol) was added slowly. The mixture was then stirred at ambient temperature for 18 h, followed by the addition of water (100 mL). The aqueous phase was extracted with CH_2Cl_2 (200 mL); the combined organic phases were dried ($MgSO_4$) and concentrated under a reduced pressure. The crude product was purified through column chromatography (SiO_2; CH_2Cl_2/hexane, 2:5) to give a pale-yellow oil.

*4.1.2.4. 5-(5-6-[3,4,5-Tris(dodecyloxy)phenyl]dithieno[3,2-b:2′,3′-a]thiophylthiophen-2-yl)thiophene-2-carbaldehyde (**8**).* A 250-mL two-neck flask containing **5** (1.1 mmol, 0.85 g), **6** (0.77 mmol, 0.21 g), and $Pd(PPh_3)_4$ (0.03 mmol, 0.026 g), in toluene (15 mL) was heated at 90 °C for 24 h. The mixture was the partitioned between CH_2Cl_2 and water. The organic phase was dried ($MgSO_4$) and concentrated under reduced pressure. The residue was purified through column chromatography (SiO_2; CH_2Cl_2/hexane, 1:1) to give a red-orange solid (0.5 g, 64.5%).

*4.1.2.5. 5-(5-6-[3,4,5-Tris(dodecyloxy)phenyl]dithieno[3,2-b:2′,3′-a]thiophenyl-2-(4-hexylthiazol-2-yl)-4-hexylthiazole-2-carbaldehyde) (**9**).* A 250-mL, two-neck flask containing **5** (0.85 g, 1.1 mmol), **7** (0.21 g, 0.77 mmol), and $Pd(PPh_3)_4$ (0.026 g, 0.03 mmol), in toluene (15 mL) was heated at 90 °C for 24 h. The mixture was partitioned between CH_2Cl_2 and water and then the organic phase was dried ($MgSO_4$) and concentrated under reduced pressure. The residue was purified through column chromatography (SiO_2; EtOAc/hexane, 1:10) to give a red-orange solid (0.5 g, 64.5%).

*4.1.2.6. 3-{6-[3,4,5-Tris(dodecyloxy)phenyl]dithieno[3,2-b:2′,3′-a] thiophene-2-yl}-2-cyanoacrylic acid (**Cpd11**).* A mixture of **4** (0.70 g,

0.08 mmol), cyanoacetic acid (0.12 g, 1.41 mmol), ammonium acetate (0.063 g, 0.08 mmol), and glacial AcOH (60 mL) was heated overnight at 110 °C with efficient stirring. The red solution was cooled to induce a precipitate, which was filtered off and thoroughly washed with water and MeOH, to give a red solid (79.8%).

*4.1.2.7. 3-{5-(5-6-[3,4,5-Tris(dodecyloxy)phenyl]dithieno[3,2-b:2′,3′-a]thiophylthiophen-2-yl)thiophenyl}-2-cyanoacrylic acid (**Cpd16**).* Prepared, using the same procedure as that described for **Cpd11**, as a dark-brown solid (73.2%).

*4.1.2.8. 3-{5-(5-6-[3,4,5-Tris(dodecyloxy)phenyl]dithieno[3,2-b:2′,3′-a]thiophyl}-2-(4-hexylthiazol-2-yl)-4-hexylthiazole-2-cyanoacrylic acid) (**Cpd22**).* Prepared, using the same procedure as that described for **Cpd11**, as a dark-brown solid (73.2%).

4.1.3. Measurement and characterizations. ^{1}H NMR spectra were recorded using a Varian unity 300 MHz spectrometer, with DMSO-d_6 and $CHCl_3$ as solvents. Elemental analyses were performed using a HERAEUS CHN–OS RAPID elemental analyzer. UV–vis absorption spectra of dilute THF solutions (10^{-5} M) were recorded using an HP G1103A spectrophotometer; photoluminescence (PL) spectra were recorded using a Hitachi F-4500 spectrophotometer. Cyclic voltammetry (CV) was performed at room temperature using a BAS 100 electrochemical analyzer, a standard three-electrode electrochemical cell, and a 0.1 M tetrabutylammonium hexafluorophosphate ($TBAPF_6$) solution (in THF), with a scanning rate of 100 mV s^{-1}. During CV measurements, the solutions were purged with N_2 for 30 s. In each case, a carbon coating rod was the working electrode, a platinum wire was the counter electrode, and a silver wire was the quasi-reference electrode; a Ag/AgCl (3 M KCl) electrode served as the reference electrode for all potentials quoted herein. The redox couple of ferrocene/ferrocenium ion (Fc/Fc^+) was used as an external standard. The corresponding HOMO and LUMO energy levels were calculated from the onset oxidation potential ($E_{ox/onset}$) and UV–vis absorption edge (E_g^{opt}), respectively. Mesophasic textures were characterized through POM using a Leica DMLP equipped with a hot stage.

4.1.3.1. XRD characterization. Synchrotron powder XRD was performed at beamline BL17A of the National Synchrotron Radiation Research Center (NSRRC), Taiwan; the wavelength of the X-rays was 1.33366 Å. The powder samples were packed into a capillary tube and heated with a heat gun, the temperature controller of which was programmed by a PC with a PID feedback system. The scattering angle, θ, was calibrated using a mixture of silver behenate and silicon.

4.1.3.2. TiO_2 paste preparation. The TiO_2 precursor and the electrode were fabricated using previously reported procedures[34] with an autoclave temperature of 240 °C. The precursor solution was prepared according to the following procedure: 0.1 M HNO_3 (430 mL) under vigorous stirring was slowly combined with $Ti(C_3H_7O)_4$ (72 mL). After hydrolysis, the mixture was heated at 85 °C in a water bath and stirred vigorously for 8 h to achieve peptization. The mixture was cooled to room temperature and the resultant colloid was filtered; the filtrate was then heated in an autoclave at 240 °C for 12 h to grow the TiO_2 particles. The colloid was cooled to room temperature and vibrated ultrasonically for 10 min. The TiO_2 colloid was concentrated to 13 wt %, followed by the addition of 30 wt % (with respect to TiO_2 weight) of poly(ethylene glycol) (PEG; MW=20,000 g mol^{-1}) to prevent the film from cracking while drying.

4.1.3.3. Device fabrication. The TiO_2 paste was deposited on a FTO glass substrate (dimensions: 0.5×0.5 cm^2) using the glass rod method. Polyester tape (3 M) was used as an adhesive on two edges of the FTO glass. The tape was removed after the TiO_2 paste had been spread on the FTO using a glass rod and then the TiO_2 paste was dried in air at room temperature for 1 h. The TiO_2-coated FTO was heated to 500 °C at a heating rate of 10 °C min^{-1} and then maintained at that temperature for 30 min before cooling to room temperature. After repeating the procedure above to control the thickness of the TiO_2 film, the final coating was performed using TiO_2 pastes containing different sizes (300 and 20 nm; 30 and 70 wt %, respectively) of light-scattering TiO_2 particles; the samples were then heated at 500 °C. The thicknesses of the TiO_2 films were measured using a profilometer (Dektak3, Veeco/Sloan Instruments). The density of each adsorbed dye was calculated from the concentration difference of each solution before and after TiO_2 film immersion. The TiO_2 electrode with a geometric area of 0.25 cm^2 was immersed overnight in a MeCN/*tert*-butanol (1:1, v/v) solution of 3×10^{-4} M *cis*-di(thiocyanato)bis(2,2′-bipyridyl-4,4′-dicarboxylato)-ruthenium(II) bis(tetrabutylammonium) (**N719**, Solaronix SA) or in a THF solution containing 3×10^{-4} M organic sensitizers. Thermally platinized FTO was used as the counter electrode; its active area was controlled to 0.36 cm^2 using adhered polyester tape having a thickness of 60 μm. After rinsing with MeCN or THF, the photoanode was placed on top of the counter electrode and tightly clipped together to form a cell. Electrolyte was injected into the space and then the cell was sealed with Torr Seal cement (Varian). The electrolyte comprised 0.5 M LiI, 0.05 M I_2, and 0.5 M 4-*tert*-butylpyridine (TBP) in MeCN. The photovoltage transients of the assembled devices were recorded using a digital oscilloscope (LeCroy, WaveSurfer 24Xs). Pulsed laser excitation was applied using a Q-switched Nd:YAG laser (Continuum, model Minilite II) operated at 532 nm, with a 1 Hz repetition rate and a 5-ns pulse width at half-height. The beam size was slightly larger than 0.5×0.5 cm^2 to cover the area of the device. The photovoltage of each device was adjusted by incident pulse energy to be 40 mV.

4.1.3.4. Device measurements. A 0.6×0.6 cm^2 cardboard mask was clipped onto the device to constrain the illumination area. Photoelectrochemical characterization of the DSSCs was performed using an Oriel Class A solar simulator (Oriel 91195A, Newport). The photocurrent–voltage characteristics of the DSSCs were recorded using a potentiostat/galvanostat (CHI650B, CH Instruments) at a light intensity of 1.0 sun, calibrated using an Oriel reference solar cell (Oriel 91150, Newport). The monochromatic quantum efficiency was recorded through a monochromator (Oriel 74100, Newport) under short-circuit conditions. The intensity of each wavelength was in the range from 1 to 3 mW cm^{-2}.

Acknowledgements

The powder XRD measurements are supported by beamline BL17A1 (charged by Dr. Jey-Jau Lee) of the National Synchrotron Radiation Research Center (NSRRC) in Taiwan. The financial supports of this project provided by the National Science Council of Taiwan (ROC) through NSC 99-2113-M-009-006-MY2, NSC 99-2221-E-009-008-MY2, and National Chiao Tung University through 97W807 are acknowledged.

References and notes

1. O'Regan, B.; Grätzel, M. *Nature* **1991**, *353*, 737–740.
2. Grätzel, M. *Nature* **2001**, *414*, 338–344.
3. Abbotto, A.; Barolo, C.; Bellotto, L.; De Angelis, F.; Grätzel, M.; Manfredi, N.; Marinzi, C.; Fantacci, S.; Yum, J. H.; Nazeeruddin, M. K. *Chem. Commun.* **2008**, 5318–5320.
4. Chen, C. Y.; Chen, J. G.; Wu, S. J.; Li, J. Y.; Wu, C. G.; Ho, K. C. *Angew. Chem., Int. Ed.* **2008**, *47*, 7342–7345.
5. Im, H.; Kim, S.; Park, C.; Jang, S. H.; Kim, C. J.; Kim, K.; Park, N. G.; Kim, C. *Chem. Commun.* **2010**, 1335–1337.

6. Tang, J.; Wu, W.; Hua, J.; Li, J.; Li, X.; Tian, H. *Energy Environ. Sci.* **2009**, *2*, 982–990.
7. Yin, J. F.; Chen, J. G.; Lu, Z. Z.; Ho, K. C.; Lin, H. C.; Lu, K. L. *Chem. Mater.* **2010**, *22*, 4392–4399.
8. Yin, J. F.; Bhattacharya, D.; Hsu, Y. C.; Tsai, C. C.; Lu, K. L.; Lin, H. C.; Chen, J. G.; Ho, K. C. *J. Mater. Chem.* **2009**, *19*, 7036–7042.
9. Wang, Z. S.; Cui, Y.; Dan-oh, Y.; Kasada, C.; Shinpo, A.; Hara, K. *J. Phys. Chem. C.* **2007**, *111*, 7224–7230.
10. Mishra, A.; Fischer, M. K. R.; Bäuerle, P. *Angew. Chem., Int. Ed.* **2009**, *48*, 2474–2499.
11. Horiuchi, T.; Miura, H.; Uchid, S. *Chem. Commun.* **2003**, 3036–3037.
12. Clifford, J. N.; Martínez-Ferrero, E.; Viterisi, A.; Palomares, E. *Chem. Soc. Rev.* **2011**, *40*, 1635–1646.
13. Hagfeldt, A.; Boschloo, G.; Sun, L. C.; Kloo, L.; Pettersson, H. *Chem. Rev.* **2010**, *110*, 6595–6663.
14. Do, K.; Kim, D.; Cho, N.; Paek, S. H.; Song, K. Y.; Ko, J. J. *Org. Lett.* **2012**, *14*, 222–225.
15. Guo, K. P.; Yan, K. Y.; Lu, X. Q.; Qiu, Y. C.; Liu, Z.; Sun, J. W.; Yan, F.; Guo, W. Y.; Yang, S. *Org. Lett.* **2012**, *14*, 2214–2217.
16. Lu, X. F.; Feng, Q. Y.; Lan, T.; Zhou, G.; Wang, Z. S. *Chem. Mater.* **2012**, *24*, 3179–3187.
17. Sahu, D.; Padhy, H.; Patra, D.; Yin, J. F.; Hsu, Y. C.; Lin, J. T.; Lu, K. L.; Wei, K. H.; Lin, H. C. *Tetrahedron* **2011**, *67*, 303–311.
18. Zhou, H. P.; Xue, P. C.; Zhang, Y.; Zhao, X.; Jia, J. H.; Zhang, X. F.; Liu, X. L.; Lu, R. *Tetrahedron* **2011**, *67*, 8477–8483.
19. Li, Y. T.; Chen, C. L.; Hsu, Y. Y.; Hsu, H. C.; Chi, Y.; Chen, B. S.; Liu, W. H.; Lai, C. H.; Lin, T. Y.; Chou, P. T. *Tetrahedron* **2010**, *66*, 4223–4229.
20. Guo, M.; Diao, P.; Ren, Y. J.; Meng, F.; Tian, H.; Cai, S. M. *Sol. Energy Mater. Sol. Cells* **2005**, *88*, 23–35.
21. Yasuda, T.; Ooi, H.; Morita, J.; Akama, Y.; Minoura, K.; Funahashi, M.; Shimomura, T.; Kato, T. *Adv. Funct. Mater.* **2009**, *19*, 411–419.
22. Yoon, S. J.; Kim, J. H.; Kim, K. S.; Chung, J. W.; Heinrich, B.; Mathevet, F.; Kim, P.; Donnio, B.; Attias, A. J.; Kim, D.; Park, S. Y. *Adv. Funct. Mater.* **2012**, *22*, 61–69.
23. Barberá, J.; Godoy, M. A.; Hidalgo, P. I.; Parra, M. L.; Ulloa, J. A.; Vergara, J. M. *Liq. Cryst.* **2011**, *38*, 679–688.
24. Rajan, Y. C.; Shellaiah, M.; Huang, C. T.; Lin, H. C.; Lin, H. C. *Tetrahedron* **2012**, *68*, 7926–7931.
25. Steckler, T. T.; Zhang, X.; Hwang, J.; Honeyager, R.; Ohira, S.; Zhang, X. H.; Grant, A.; Ellinger, S.; Odom, S. A.; Sweat, D.; Tanner, D. B.; Rinzler, A. G.; Barlow, S.; Brédas, J. L.; Kippelen, B.; Marder, S. R.; Reynolds, J. R. *J. Am. Chem. Soc.* **2009**, *131*, 2824–2826.
26. Chen, C. H.; Hsu, Y. C.; Chou, H. H.; Thomas, K. R. J.; Lin, J. T.; Hsu, C. P. *Chem.—Eur. J.* **2010**, *16*, 3184–3193.
27. Heredia, D.; Natera, J.; Gervaldo, M.; Otero, L.; Fungo, F.; Lin, C. Y.; Wong, K. T. *Org. Lett.* **2010**, *12*, 12–15.
28. Yang, H. Y.; Yen, Y. S.; Hsu, Y. C.; Chou, H. H.; Lin, J. T. *Org. Lett.* **2010**, *12*, 16–19.
29. Huang, J. H.; Ho, Z. Y.; Kekuda, D.; Chang, Y.; Chu, C. W.; Ho, K. C. *Nanotechnology* **2009**, *20*, 025202 (1–9).
30. Ozturk, T.; Ertasb, E.; Mertc, O. *Tetrahedron* **2005**, *61*, 11055–11077.
31. Qin, H.; Wenger, S.; Xu, M. F.; Gao, F. F.; Jing, X. Y.; Wang, P.; Zakeeruddin, S. M.; Grätzel, M. *J. Am. Chem. Soc.* **2008**, *130*, 9202–9203.
32. Zhang, S. M.; Guo, Y. L.; Fan, H. J.; Liu, Y.; Chen, H. Y.; Yang, G. W.; Zhan, X. W.; Liu, Y. Q.; Li, Y. F.; Yang, Y. *J. Polym. Sci., Part A: Polym. Chem.* **2009**, *47*, 5498–5508.
33. Li, K. C.; Huang, J. H.; Hsu, Y. C.; Huang, P. J.; Chu, C. W.; Lin, J. T.; Ho, K. C.; Wei, K. H.; Lin, H. C. *Macromolecules* **2009**, *42*, 3681–3693.
34. Wang, L.; Chen, Q.; Pan, G. B.; Wan, L. J.; Zhang, S.; Zhan, X.; Northrop, B. H.; Stang, P. J. *J. Am. Chem. Soc.* **2008**, *130*, 13433–13441.
35. Huo, L.; Hou, J.; Zhang, S.; Chen, H. Y.; Yang, Y. *Angew. Chem., Int. Ed.* **2010**, *8*, 1500–1503.
36. Li, W. S.; Yamamoto, Y.; Fukushima, T.; Saeki, A.; Seki, S.; Tagawa, S.; Masunaga, H.; Sasaki, S.; Takata, M.; Aida, T. *J. Am. Chem. Soc.* **2008**, *130*, 8886–8887.
37. Zhang, S. M.; Guo, Y. L.; Wang, L.; Li, Q. K.; Zheng, K.; Zhan, X. W.; Liu, Y. Q.; Liu, R. Q.; Wan, L. J. *J. Phys. Chem. C* **2009**, *113*, 16232–16237.
38. He, J. X.; Wu, W. J.; Hua, J. L.; Jiang, Y. H.; Qu, S. Y.; Li, J.; Long, Y. T.; Tian, H. *J. Mater. Chem.* **2011**, *21*, 6054–6062.
39. Mann, J. R.; Gannon, M. K.; Fitzgibbons, T. C.; Detty, M. R.; Watson, D. F. *J. Phys. Chem. C* **2008**, *112*, 13057–13061.
40. Chen, K. F.; Hsu, Y. C.; Wu, Q.; Yeh, M. C. P.; Sun, S. S. *Org. Lett.* **2009**, *11*, 377–380.
41. Baheti, A.; Tyagi, P.; Thomas, K. R. J.; Hsu, Y. C.; Lin, J. T. *J. Phys. Chem. C* **2009**, *113*, 8541–8547.
42. Chaurasia, S.; Chen, Y. C.; Chou, H. H.; Wen, Y. S.; Lin, J. T. *Tetrahedron* **2012**, *68*, 7755–7762.
43. Tian, H.; Yang, X.; Chen, R.; Zhang, R.; Hagfeldt, A.; Sun, L. *J. Phys. Chem. C* **2008**, *112*, 11023–11033.
44. Lin, L. Y.; Tsai, C. H.; Lin, F.; Huang, T. W.; Chou, S. H.; Wu, C. C.; Wong, K. T. *Tetrahedron* **2012**, *68*, 7509–7516.
45. Higashijima, S.; Miura, H.; Fujita, T.; Kubota, Y.; Funabiki, K.; Yoshida, T.; Matsui, M. *Tetrahedron* **2011**, *34*, 6289–6293.
46. Cho, N.; Choi, H.; Kim, D.; Song, K.; Kang, M. S.; Kang, S. O.; Ko, J. *Tetrahedron* **2009**, *31*, 6236–6243.
47. Lu, G.; Usta, H.; Risko, C.; Wang, L.; Facchetti, A.; Ratner, M.; Marks, T. J. *J. Am. Chem. Soc.* **2008**, *130*, 7670–7685.
48. Koppe, M.; Scharber, M.; Brabec, C.; Duffy, W.; Heeney, M.; McCulloch, I. *Adv. Funct. Mater.* **2007**, *17*, 1371–1376.
49. Huang, C. Y.; Hsu, Y. C.; Chen, J. G.; Suryanarayanan, V.; Lee, K. M.; Ho, K. C. *Sol. Energy Mater. Sol. Cells* **2006**, *90*, 2391–2397.
50. Li, H.; Jiang, P.; Yi, C.; Li, C.; Liu, S. X.; Tan, S. T.; Zhao, B.; Braun, J.; Meier, W.; Wandlowski, T.; Decurtins, S. *Macromolecules* **2010**, *43*, 8058–8062.
51. Zhang, M.; Fan, H.; Guo, X.; He, Y.; Zhang, Z.; Min, J.; Zhang, J.; Zhao, G.; Zhan, X. W.; Li, Y. F. *Macromolecules* **2010**, *43*, 5706–5712.